

FAULT MONITORING AND FAULT RECOVERY CONTROL FOR POSITION-MOORED VESSELS

SHAOWJI FANG *, MOGENS BLANKE **,*

* Centre for Ships and Ocean Structures
Norwegian University of Science and Technology, Otto Niensens Vei 10, NO 7491 Trondheim, Norway
e-mail: shaoji.fang@ntnu.no

** Automation and Control Group, Department of Electrical Engineering
Technical University of Denmark, Elektrovej build. 326, DK 2800 Kgs Lyngby, Denmark
e-mail: mb@elektro.dtu.dk

This paper addresses fault-tolerant control for position mooring of a shuttle or floating production storage and offloading vessels. A complete framework for fault diagnosis is presented. A loss of a sub-sea mooring line buoyancy element and line breakage are given particular attention, since such failures might cause high-risk abortion of an oil-loading operation. With significant drift forces from waves, non-Gaussian elements dominate forces and the residuals designed for fault diagnosis. Hypothesis testing is designed using dedicated change detection for the type of distribution encountered. A new position recovery algorithm is proposed as a means of fault accommodation in order to keep the mooring system in a safe state, despite faults. The position control is shown to be capable of accommodating serious failures and preventing breakage of a mooring line, or a loss of a buoyancy element, from causing subsequent failures. Properties of the detection and fault-tolerant control algorithms are demonstrated by high fidelity simulations.

Keywords: fault diagnosis, fault-tolerant control, fault recovery, position mooring, non-Gaussian change detection.

1. Introduction

With oil and gas exploration going into deeper waters and harsher environments, Position-Mooring (PM) systems are encountering more challenges with regard to mechanical reliability, automatic control and associated safety aspects. For thruster-assisted position mooring, the main objective is to maintain the vessel's position within a limited region and keep the vessel on the desired heading such that the external environmental load is minimised (Strand *et al.*, 1998; Aamo and Fossen, 2001). In extreme weather, the main objective changes to that of ensuring that mooring lines avoid breakage (Nguyen and Sørensen, 2007; Berntsen *et al.*, 2008a).

The safety of dynamic positioning is a prime concern in the marine industry, and regulations are made to prevent that faults in equipment cause accidents at the system level (DNV, 2008b). In position mooring, accident consequences need be analysed for line breakage and the loss of one or more Mooring Line Buoyancy Elements (MLBEs). Such analysis has traditionally been based solely on the

reliability analysis of mechanical structures, with studies of risk of fatigue damage or line breakage under extreme conditions as the essential means of analysis (Gao and Moan, 2007).

Since thrusters are also available on the types of vessels considered, the automatic control part has been receiving increased attention for reasons of potential contributions to safety. A non-linear controller was proposed by Berntsen *et al.* (2006), who formulated a structural reliability index and a controller to prevent a mooring line from getting into a zone of low reliability. A switching controller was used by Nguyen and Sørensen (2009) for thruster-assisted position mooring. Mooring line breakage was prevented by detecting a change in the environment and switching between dedicated controllers. Systematic fault-tolerant control was studied for station keeping of a marine vessel by Blanke (2005), who validated a structure-graph approach to fault diagnosis and control reconfiguration by sea tests. Nguyen and Sørensen (2007) extended this study to position mooring and suggested off-line fault-accommodation design of a bank of controllers.

Failure of mooring line buoyancy elements was not considered in these previous studies.

The purpose of this paper is to widen fault-tolerant control design for position-mooring systems to include a loss of mooring line buoyancy elements and to enhance the fault-tolerant control strategy in the case of mooring line breakage. Investigating control-system topology by structure-graph analysis, diagnosis system design is extended to include buoyancy elements on mooring lines. Residuals are shown to be non-Gaussian, due to the nature of drift forces from waves, and a dedicated change-detection and hypothesis test is designed for the particular distributions at hand. A novel algorithm is suggested for fault accommodation that is capable of avoiding breakage of further mooring lines, even if one line is broken or a buoyancy element has been lost. Simulations illustrate how the new position algorithm prevents mooring line tension from exceeding a critical level after either of these two failures.

The remainder of this paper is organised as follows. Section 2 addresses the modelling of the position-moored vessel. Section 3 presents fault diagnosis and change detection. The optimal position algorithm in fault accommodation is presented in Section 4. The proposed algorithm is validated by simulations in Section 5, and conclusions are drawn in Section 6.



Fig. 1. Typical position-mooring system.

2. System modelling

The purpose of modelling is to obtain information to design Fault Detection and Isolation (FDI) modules for essential faults and to give the prerequisites for control re-configuration design when faults occur.

The basic configuration of a position-mooring system is presented in Fig. 2. The figure shows the equipment demanded for DYNPOS-AUTR class DP (DNV, 2008a), which is the most reliable system configuration according to DNV classes, shown in Table 1. There are redundant thrusters, three position measurement systems (two GPS

Table 1. Sensor requirement of different DP classifications.

Sensor number	AUTS	AUT	AUTR
N_{pos}	1	2	3
N_{wind}	1	1	2
N_{gyro}	1	1	3
N_{vrs}	1	1	3

and one hydro-acoustic position unit (HPS)), two wind sensors, three gyro compasses and three Vertical Reference Sensors (VRS). Relative velocity through the water is measured by the ship's log and Inertial Measurement Unit (IMU). Meanwhile, the mooring line tensions are monitored by the Tension Measurement Equipment (TME).

Table 2 shows the list of symbols, and the block diagram in Fig. 2 illustrates the topology of function blocks in a position-mooring system. A typical position-mooring system is shown in Fig. 1, along with two reference frames: the Earth-Fixed Frame (EFF) and the Body-Fixed Frame (BFF), with the origin located at the Centre Of the Turret (COT), where all the mooring lines are attached to the vessel.

Table 2. List of symbols.

symbol	Explanation
h_1, h_2, h_3	yaw angle measurements
$\psi, \dot{\psi}$	yaw angle and yaw rate
$\mathbf{p}_{G1}, \mathbf{p}_{G2}, \mathbf{p}_{H1}$	position measurements in EFF
$\mathbf{p}, \dot{\mathbf{p}}$	vessel position and velocity in EFF
$\mathbf{q}_1, \mathbf{q}_2, \mathbf{q}_3$	vertical reference measurements
z, ϕ, θ	vessel heave, roll and pitch
$\mathbf{w}_{m1}, \mathbf{w}_{m2}, \mathbf{c}_m$	wind and current measurements
$\mathbf{v}_w, \mathbf{v}_c$	wind and current velocity
\mathbf{T}_{wave}	wave force
\mathbf{T}_{mbi}	mooring line tension
\mathbf{T}_{moi}	MLBE force
\mathbf{T}_{momi}	mooring line tension measurement
\mathbf{v}	vessel velocity in BFF
\mathbf{v}_m	velocity measurement in BFF
u_1, u_2, \dots, u_k	thruster input
T_1, T_2, T_3	thruster force

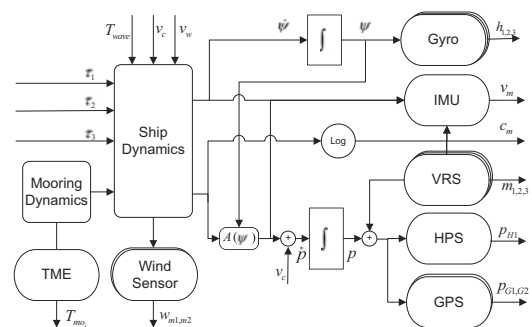


Fig. 2. Ship dynamics and sensor measurements.

Structural analysis considers a model of a system made by a set of constraints, $\mathbf{C} = \{a_1, \dots, a_i, c_1, \dots, c_i, d_1, \dots, d_i, m_1, \dots, m_i\}$, which are applied to a set of variables $\mathbf{X} = X \cup K$. X denotes the set of unknown variables, $K = K_i \cup K_m$ are known variables: measurements (K_m), control input (K_i), etc. Variables are constrained by the physical laws applied to a particular unit. a_i denotes the constraint of thruster input, c_i is the algebraic constraint, d_i denotes the differential constraint, m_i are the measurements. With the k thrusters and n mooring lines, the constraints and variables for PM are

$$\begin{aligned}
 a_1 : & \quad T_1 = g_t(u_1, u_2, \dots, u_k), \\
 a_2 : & \quad T_2 = g_l(u_1, u_2, \dots, u_k), \\
 a_3 : & \quad T_3 = g_r(u_1, u_2, \dots, u_k), \\
 c_1 : & \quad \mathbf{M}\dot{\mathbf{v}} = \mathbf{H}_{xy}\mathbf{T}[T_1, T_2, T_3]^\top \\
 & \quad + [g_w^x(v_w)g_w^y(v_w)]^\top \\
 & \quad + \sum_{j=1}^n \mathbf{A}_{mo}^{xy}(\mathbf{p}, \psi)\mathbf{T}_{moi}^{xy}(\mathbf{T}_{moi}) \\
 & \quad - \mathbf{D}[\mathbf{v} \quad \dot{\psi}]^\top + \mathbf{H}_{xy}\mathbf{T}_{wave}, \\
 c_2 : & \quad \mathbf{I}_{zz}\ddot{\psi} = \mathbf{H}_\psi\mathbf{T}[T_1, T_2, T_3]^\top + g_w^\psi(v_w) \\
 & \quad + \sum_{j=1}^n \mathbf{A}_{mo}^\psi(\mathbf{p}, \psi)\mathbf{T}_{moi}^\psi(\mathbf{T}_{moi}) \\
 & \quad + \mathbf{H}_\psi\mathbf{T}_{wave}, \\
 c_3 : & \quad \dot{\mathbf{p}} = \mathbf{A}_{ve}(\psi)\mathbf{v} + \mathbf{v}_c, \\
 c_4 : & \quad \mathbf{p}_{G1} = \mathbf{p} + \mathbf{R}(\phi, \theta, \psi)\mathbf{l}_{G1}, \\
 c_5 : & \quad \mathbf{p}_{G2} = \mathbf{p} + \mathbf{R}(\phi, \theta, \psi)\mathbf{l}_{G2}, \\
 c_6 : & \quad \mathbf{p}_{H1} = \mathbf{p} + \mathbf{R}(\phi, \theta, \psi)\mathbf{l}_{H1}, \\
 c_{2i+5} : & \quad \mathbf{T}_{moi} = g_{mo}(\mathbf{p}, \psi, \mathbf{T}_{mbi}), \\
 c_{2i+6} : & \quad \mathbf{T}_{mbi} = g_{mb}(\mathbf{p}, \psi), \\
 d_1 : & \quad \dot{\mathbf{v}} = \frac{\partial}{\partial t}\mathbf{v}, \\
 d_2 : & \quad \dot{\mathbf{p}} = \frac{\partial}{\partial t}\mathbf{p}, \\
 d_3 : & \quad \dot{\psi} = \frac{\partial}{\partial t}\psi, \\
 d_4 : & \quad \ddot{\psi} = \frac{\partial}{\partial t}\dot{\psi}, \\
 m_{1..m_3} : & \quad h_{1..3} = \psi, \\
 m_4 : & \quad \mathbf{p}_{G1}^m = \mathbf{p}_{G1}, \\
 m_5 : & \quad \mathbf{p}_{G2}^m = \mathbf{p}_{G2}, \\
 m_6 : & \quad \mathbf{p}_{H1}^m = \mathbf{p}_{H1}, \\
 m_{7..m_9} : & \quad \mathbf{q}_{1..3} = [z \quad \phi \quad \theta], \\
 m_{10} : & \quad \mathbf{v}_m = \mathbf{v}, \\
 m_{11,12} : & \quad \mathbf{w}_{m1,m2} = \mathbf{v}_w,
 \end{aligned}$$

$$\begin{aligned}
 m_{13} : & \quad \mathbf{c}_m = \mathbf{v}_c, \\
 m_{13+i} : & \quad \mathbf{T}_{momi} = \mathbf{T}_{moi},
 \end{aligned}$$

where \mathbf{M} is the mass matrix including added mass, \mathbf{D} is the damping matrix, \mathbf{I}_{zz} is the inertia moment for yaw, \mathbf{T} is the thruster configuration matrix, \mathbf{H}_{xy} is the projection matrix for surge and sway, \mathbf{H}_ψ is that for yaw, \mathbf{A}_{mo}^{xy} , \mathbf{A}_{mo}^ψ is a transformation matrix for horizontal mooring line tension from the Earth-fixed to the body-fixed frame, $\mathbf{A}_{ve}(\psi)$ is a transformation matrix for vessel velocity from the Earth-fixed to the body-fixed frame, $\mathbf{R}(\phi, \theta, \psi)$ is the transformation from a position reference system to the vessel coordinate origin, and $g_w^x(v_w)$, $g_w^y(v_w)$, $g_w^\psi(v_w)$ are the wind forces in surge, sway and the moment in yaw.

Categorising variables in the constraints as belonging to the sets X (unknown), K_i (input) and K_m (measurements), the variables are separated as

$$\begin{aligned}
 X &= \{T_1, T_2, T_3, \mathbf{T}_{mbi}, \mathbf{T}_{moi}, \mathbf{T}_{wave}, \mathbf{p}_{G1}, \mathbf{p}_{G2}, \\
 & \quad \mathbf{p}_{H1}, \mathbf{v}, \dot{\mathbf{v}}, \psi, \dot{\psi}, \ddot{\psi}, \mathbf{p}, \dot{\mathbf{p}}, \theta, \phi, \mathbf{v}_c, \mathbf{v}_w\}, \\
 K_i &= \{u_1, u_2, \dots, u_k\}, \\
 K_m &= \{h_1, h_2, h_3, \mathbf{p}_{G1}^m, \mathbf{p}_{G2}^m, \mathbf{p}_{H1}^m, \mathbf{q}_1, \\
 & \quad \mathbf{q}_2, \mathbf{q}_3, \mathbf{v}_m, \mathbf{w}_{m1}, \mathbf{w}_{m2}, \mathbf{c}_m, \mathbf{T}_{momi}\}.
 \end{aligned}$$

The modelling here presents the normal behaviour, and diagnostic algorithms will be designed to detect deviation from the norm (Blanke *et al.*, 2006), where the occurrence of full or partial failure of mooring lines can be detected and counteracted by thruster-assisted position control.

Nonlinear bifurcation phenomena that could occur when second order wave forces interact with the dynamics of a moored system are not considered. Boundary conditions for these particular nonlinear phenomena were determined by Garza-Rios and Bernitsas (1996).

3. Fault diagnosis and change detection

3.1. Structure analysis. A structure-graph approach is usually employed to obtain system analytical redundancy relations for FDI. With this technique, functional relations between measured and control variables can be used without being explicitly formulated. SaTool is software developed for this technique and a structure graph can be easily created, even for implicit nonlinear constraints (Blanke, 2005).

Structural analysis finds the over-determined subsystem and, for the present system, finds a set of $8 + i$ parity relations where i is the number of mooring lines. These parity relations can be used as residual generators for fault detection in the system. A deviation from the norm of a constraint, i.e., a fault, will affect a parity relation if this relation is constructed using the constraint. Considering

mooring line faults, the result is i such relations:

$$r_{5+i} = m_{13+i}(\mathbf{T}_{\text{momi}}, c_{2i+5}(c_6(m_3(h_3), m_9(\mathbf{q}_3), m_6(\mathbf{P}_{H1}^m)), m_3(h_3), c_{2i+6}(c_6(m_3(h_3), m_9(\mathbf{q}_3), m_6(\mathbf{P}_{H1}^m)), m_3(h_3)))).$$

If a fault affects the residual vector, the fault is structurally detectable. If a particular fault has a unique pattern in the residual vector's elements, it is structurally isolable. In the presence of only one fault, structurally isolable constraints are $(c_4, m_1, m_2, m_3, m_7, m_8, m_9)$ while the detectable constraints are $(c_3, c_5, c_6, c_{2i+5}, c_{2i+6}, d_2, m_5, m_6, m_{10}, m_{11}, m_{12}, m_{13}, m_{13+i})$.

3.2. Change detection. After the design of the residual generators, hypothesis testing needs to be designed to detect the change of the residual. For violation of constraints c_{2i+5}, c_{2i+6} , changes will be structurally visible on residuals r_{5+i} .

The design intention of the Mooring Line Buoyancy Element (MLBE) is to reduce the static force and dynamic motion of the mooring system (Mavrakos *et al.*, 1996). Buoyancy elements need be designed suitably, otherwise adverse effects could occur. The loss of a buoyancy element would cause a force deviation on the mooring line, and a similar effect would also occur in the event of the line breaking. This deviation is reflected on the residuals r_{5+i} , and the detection algorithm of the force deviation in r_{5+i} could be found in the work of Nguyen *et al.* (2007) with a fault that one mooring line is broken. Nguyen *et al.* (2007) assume a Gaussian distribution of this residual and design a CUMSUM detector for the tension deviation.

However, all of these residuals should be non-Gaussian distributed due to nonlinear vessel dynamics and the nature of wave drift forces. First order wave forces will generally give Gaussian distributions and the slowly varying drift forces can be calculated to give Rayleigh-distributed forces, if one just assumes that forces arise as the amplitude of a sum of Gaussian elements. A more accurate assessment of the distribution of forces on a moored tanker was the subject of studies including the one by Wang and Xu (2008), where forces and moments affecting a Floating Production, Storage and Off-loading (FPSO) vessel were computed by the near-field method based on direct-pressure integration. Wang and Tan (2008) modelled the response of a moored vessel excited by slowly varying non-Gaussian wave drift forces as a continuous Markov process. Næss (1986) as well as Kim and Dick (1989) studied the statistical distribution of slowly varying drift forces and moments. The distribution of these forces and moments enters into the expressions of the residual we generate for fault diagnosis, but since residual generation involves dynamics and filtering by the residual generator, the amplitude distribution of residuals is not the same as

the amplitude distributions of wave drift forces and moments, although, of course, they are related. The problem of finding the distribution of residuals by analytical means is not within the scope of the present paper. Instead, we turn to simulations and an approximation to observed distributions with, and without, faults being present.

The distribution of the residual r_{5+i}/T_{ci} is presented in Fig. 3 and this also shows an approximating Rayleigh distribution. Note that T_{ci} is the critical mooring line tension. The approximation is not a perfect match to the residual obtained from simulations, but for detection of a change, it is clearly better than commonly applied detection algorithms for Gaussian-distributed residuals (Kay, 1998).

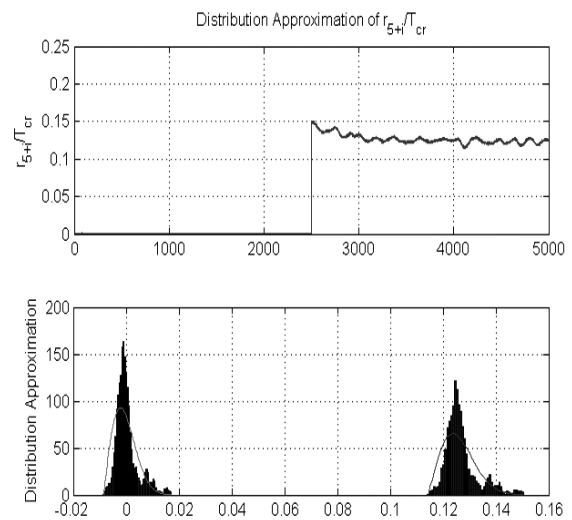


Fig. 3. Time history of r_{5+i}/T_{ci} and approximation of amplitude histograms by Rayleigh distributions. A buoyancy element is lost at $t = 2500$ s. Sea conditions: wave height $h_{1/3} = 7$ m, wave period $T_p = 10.5$ s.

In Fig. 3, the mean value of the residual r_{5+i}/T_{ci} is shifted away from zero, both with and without faults being present. A shifted Rayleigh density function replicates this behaviour. Considering that relationship between the variance of the Rayleigh-distributed signal σ_R and the variance of the underlying Gaussian signal σ is $\sigma_R^2 = (2 - \frac{\pi}{2})\sigma^2$, the shifted Rayleigh density function is expressed as follows, where σ_R^2 is the variance and μ_R is its mean value:

$$p(z(k)) = \frac{(4 - \pi)(z(k) - \mu_R + \frac{\sqrt{\sigma_R^2 \pi}}{\sqrt{4 - \pi}})}{2\sigma_R^2} \cdot \exp \left[- \frac{(\sqrt{4 - \pi}(z(k) - \mu_R) + \sqrt{\sigma_R^2 \pi})^2}{4\sigma_R^2} \right]$$

for

$$z(k) \geq \mu_R - \frac{\sqrt{\sigma_R^2 \pi}}{\sqrt{4 - \pi}}.$$

Detection of a change is done using a Rao test (Kay, 1998), which is the suitable detector for the mean value change in a non-Gaussian noise. The hypothesis for this case is then given by

$$\begin{aligned} H_0 : z(k) &= \mu_0 + w(k), & k = 0, 1, \dots, N - 1, \\ H_1 : z(k) &= \mu_1 + w(k), & k = 0, 1, \dots, N - 1, \end{aligned}$$

where the signal $w(k)$ is Rayleigh, and μ_0 and μ_1 are the mean values before and after a change. The test statistics for the Rao test can now be written as

$$T_R(z) = \frac{\left(\frac{\partial \ln(p(z, \mu_R))}{\partial \mu_R}\right) \Big|_{\mu_R = \hat{\mu}}^2}{I(\hat{\mu})} > \gamma, \quad (1)$$

where $\hat{\mu}$ is an estimate of the signal's mean value, $I(\hat{\mu})$ is the Fisher information, and the probability density function $p(z, \mu_R)$ is

$$\begin{aligned} p(z, \mu_R) &= \frac{(4 - \pi)^N \prod_{k=0}^{N-1} \left(z(k) - \mu_R + \frac{\sqrt{\sigma_R^2 \pi}}{\sqrt{4 - \pi}}\right)}{2^N \sigma_R^{2N}} \\ &\cdot \exp\left(-\frac{\sum_{k=0}^{N-1} \left(\sqrt{4 - \pi} (z(k) - \mu_R) + \sqrt{\sigma_R^2 \pi}\right)^2}{4\sigma_R^2}\right). \end{aligned} \quad (2)$$

The partial derivative of the logarithm of the probability density function is found as

$$\begin{aligned} \frac{\partial \ln(p(z, \mu_R))}{\partial \mu_R} &= \frac{4 - \pi}{2\sigma_R^2} \sum_{n=0}^{N-1} \left(z(k) - \mu_R + \sqrt{\frac{\pi\sigma_R^2}{4 - \pi}}\right) \\ &- \frac{2\sigma_R^2}{4 - \pi} \sum_{n=0}^{N-1} \frac{1}{z(k) - \mu_R + \sqrt{\frac{\pi\sigma_R^2}{4 - \pi}}}. \end{aligned} \quad (3)$$

The Fisher information with the Rayleigh distribution is found to be

$$\begin{aligned} I(\mu_R) &= \frac{N(4 - \pi)}{2\sigma_R^2} \sqrt{\frac{\pi\sigma_R^2}{4 - \pi}} \\ &+ \frac{2\sigma_R^2}{(4 - \pi)^2} \sum_{n=0}^{N-1} \frac{1}{\left(\sqrt{4 - \pi} (z(k) - \mu_R) + \sqrt{\pi\sigma_R^2}\right)^2}, \end{aligned} \quad (4)$$

where μ_R is estimated online as $\mu_R = \hat{\mu}$, and σ_R is assumed to be unchanged. Finally the test statistics $T_R(z)$ can be deduced based on Eqn. (1) with Eqns. (3) and (4).

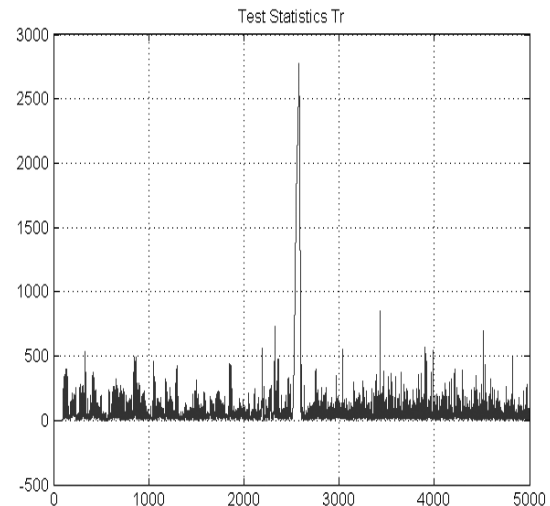


Fig. 4. Test statistics with loss of a buoy at $t = 2500$ s.

The above detector derived from Eqns. (1)–(4) is only available for data larger than zero and the Rayleigh density function is shifted to have the mean value μ_R . The data now need to satisfy

$$\epsilon(k) = \max\left(z(k) - \mu_R + \sqrt{\frac{\sigma_R^2 \pi}{4 - \pi}}, 0\right). \quad (5)$$

In order to be able to use the same threshold for all tests, data are normalised and the result of the test statistics is shown in Fig. 4.

In Fig. 4, the test statistics show a case that the loss of one buoy is simulated to happen at time $t = 2500$ s. In the test statistics, there is a sharp increase at the time $t = 2500$ s, and this event can be rapidly detected.

The change-detection method applied here is based on residuals generated in symbolic form through structural analysis, and subsequently deduced in analytical form using the system constraints. Some faults will not be isolable through this approach, but active fault isolation can help isolate faults by applying dedicated test signals to thrusters once a fault has been detected. Active fault diagnosis was analysed for Gaussian residuals by Poulsen and Niemann (2008), and the application on a water for injection system refers to Laursen *et al.* (2008). The structural conditions were obtained by Blanke and Staroswiecki (2006), and a detailed design and test on a position-moored tanker was presented by Nguyen and Blanke (2009) making use of active diagnosis.

4. Fault tolerant control

4.1. Controller design. The control objective is to maintain the vessel's position in a limited region and keep the vessel on the desired heading such that the external environmental load is minimised. Another objective is to avoid line breakage and keep the mooring system in a safe state. An optimal position algorithm is designed to meet the second objective.

The control action for PM also aims to counteract the low-frequency part of vessel motion caused by current and wind as well as second order mean and slowly varying wave loads. The specific function of control action in PM can be found in the work of Nguyen and Sørensen (2007). For controller design, it is common to use multi-variable PID control in PM systems with the structure

$$\begin{aligned} \tau_{thr} = & -\mathbf{K}_i \mathbf{R}^T(\psi) \int \hat{\boldsymbol{\eta}}_e dt \\ & - \mathbf{K}_p \mathbf{R}^T(\psi) \hat{\boldsymbol{\eta}}_e - \mathbf{K}_d \hat{\boldsymbol{\nu}}_e, \end{aligned} \quad (6)$$

where $\hat{\boldsymbol{\eta}}_e = \hat{\boldsymbol{\eta}} - \boldsymbol{\eta}_d$ and $\hat{\boldsymbol{\nu}}_e = \hat{\boldsymbol{\nu}} - \boldsymbol{\nu}_d$ are the position and velocity errors, $\boldsymbol{\eta}_d$ and $\boldsymbol{\nu}_d$ the desired position and velocity vectors, and \mathbf{K}_d , \mathbf{K}_i and $\mathbf{K}_p \in \mathbb{R}^{3 \times 3}$ are the non-negative controller gain matrices. Here ψ is the measured heading angle and $\mathbf{R}(\psi)$ is the rotation matrix from the body-fixed frame to the Earth-fixed frame, which can be found in the work of Fossen (2002). However, for certain faults, this controller cannot provide sufficiently good control. The nonlinear backstepping technique applied into the offshore vessel is found in the work of Witkowska *et al.* (2007), and further research about sliding mode control on marine vessels is found in that by Tomera (2010).

4.2. Optimal position chasing. To maintain all mooring lines in a safe state, an optimal position algorithm is proposed here. A position-mooring system is restricted to a safety region, which is normally defined from considering the static mooring line tension (Nguyen and Sørensen, 2007). A reliability index was also used to evaluate this region (Berntsen *et al.*, 2008a). This section proposes a new optimal position algorithm based on the mooring line tension for use in online fault-tolerant control.

First, a reference model is used to obtain smooth transitions in chasing the optimal position set-point. This reference model refers to Fossen (2002) and produces a smooth position reference which is the input to the position control law in Eqn. (6).

An optimal set-point is achieved through a quadratic object function based on each mooring line horizontal tension:

$$L(T_{m1}, T_{m2}, \dots, T_{mn}) = \sum_{i=1}^n \alpha_i T_{mi}^2, \quad (7)$$

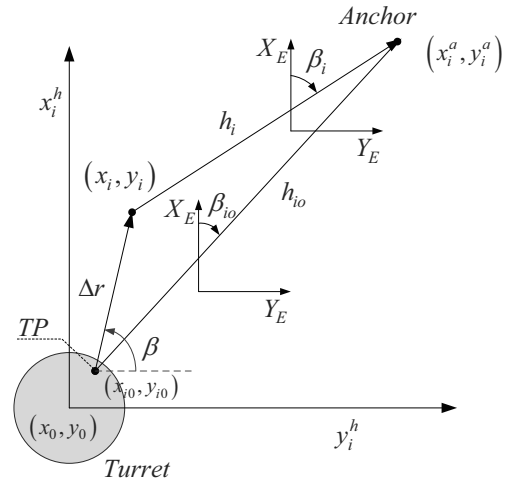


Fig. 5. Coordinate definitions for a mooring line.

where T_{mi} is the i -th horizontal mooring line tension and α_i a weighting factor. For the mooring system fixed on a turret, motion of a mooring line is shown in Fig. 5. The i -th mooring line is fixed on the sea floor with an anchor at point (x_i^a, y_i^a) . At the other end, the mooring line is connected to the turret at Terminal Point (TP) (x_{i0}, y_{i0}) , and the centre of the turret is at point (x_o, y_o) . From the point (x_{i0}, y_{i0}) to the point (x_i, y_i) , the terminal point moves with distance Δr and direction β . Meanwhile, the length of the mooring is changed from h_{i0} to h_i , and the angle of the mooring in the Earth-fixed frame is changed from β_{i0} to β_i . For the mooring system connected to a turret, the terminal point is assumed to be connected in the turret's centre and the body-fixed frame is set at the centre of the turret. Thus Δr also denotes the vessel's change in position and β denotes the change in direction.

The horizontal mooring line tension T_i at the point (x_i, y_i) can be expressed as a function of the in-plane increment of the surface vessel position Δr and the direction β :

$$\begin{aligned} T_i = T_{oi} + c_i \Delta h = T_{oi} - c_i \Delta r \cos(90^\circ - \beta - \beta_{oi}) \\ = T_{oi} - c_i \Delta r \sin(\beta + \beta_{io}), \end{aligned}$$

where T_{oi} is the tension in the working point (x_o, y_o) and c_i is the incremental stiffness tension at the present instantaneous working point according to Strand *et al.* (1998).

The optimal position algorithm adjusts the optimal vessel set-point with the variation of the mooring line tensions. One application is that mooring lines lie in a zone where there is risk of breakage. Evaluation for horizontal mooring line tension could then be $T_{mi} = T_{ci} - T_i$ once the i -th mooring line has a risk beyond the critical tension T_{ci} . Alternatively, the weighting coefficient w_i is adjusted to emphasise the importance of a specific mooring line. In the case of the faulty condition, for example, lost MLBE and subsequent mooring line breakage, this algorithm is

very useful. In addition, according to the regulation of the class society (DNV, 2008b), if the mooring lines used by a vessel differ, the safety of the system must be checked, and this can also be done by utilising this approach. Thus, with this algorithm, not only prevention of mooring line breakage can be analysed, but it is also possible to derive control actions that achieve safe behaviour in real-life situations.

With a simplified notation, the objective function (cost function) for all mooring lines in a region of risk is

$$L(T_{m1}, T_{m2}, \dots, T_{mn}) = \sum_{i=1}^n \alpha_i T_{mi}^2 = \sum_{i=1}^n \alpha_i (T_{ci} - T_i)^2. \quad (8)$$

By solving the equations where the partial derivative of Eqn. (8) with respect to the optimal increment of the vessel position and the optimal direction of this increment are set to zero, the minimum value of the object function is identified. The optimal increment of vessel position Δr and the optimal direction of this increment β^o is found to be

$$\Delta r = \frac{K_{11} \sin \beta^o + K_{12} \cos \beta^o}{K_{21} \sin^2 \beta^o + 2K_{22} \sin \beta^o \cos \beta^o + K_{23} \cos^2 \beta^o},$$

$$\beta^o = \tan^{-1} \frac{K_{11} K_{23} - K_{12} K_{22}}{K_{21} K_{12} - K_{11} K_{22}},$$

where

$$K_{11} = \alpha_1 (T_{c1} - T_{o1}) c_1 \cos \beta_{1o} + \alpha_2 (T_{c2} - T_{o2}) c_2 \cos \beta_{2o} + \dots + \alpha_n (T_{cn} - T_{on}) c_n \cos \beta_{no},$$

$$K_{12} = \alpha_1 (T_{c1} - T_{o1}) c_1 \sin \beta_{1o} + \alpha_2 (T_{c2} - T_{o2}) c_2 \sin \beta_{2o} + \dots + \alpha_n (T_{cn} - T_{on}) c_n \sin \beta_{no},$$

$$K_{21} = \alpha_1 c_1^2 \cos^2 \beta_{1o} + \alpha_2 c_2^2 \cos^2 \beta_{2o} + \dots + \alpha_n c_n^2 \cos^2 \beta_{no},$$

$$K_{22} = \alpha_1 c_1^2 \sin \beta_{1o} \cos \beta_{1o} + \alpha_2 c_2^2 \sin \beta_{2o} \cos \beta_{2o} + \dots + \alpha_n c_n^2 \sin \beta_{no} \cos \beta_{no},$$

$$K_{23} = \alpha_1 c_1^2 \sin^2 \beta_{1o} + \alpha_2 c_2^2 \sin^2 \beta_{2o} + \dots + \alpha_n c_n^2 \sin^2 \beta_{no}.$$

Finally, in the general three-dimensional case, the updated vessel position and heading set-point become

$$\eta = \eta_o + \Delta r [\cos \beta^o \quad \sin \beta^o \quad 0]^T. \quad (9)$$

5. Simulation

The purpose of this simulation is to validate the proposed fault-tolerant control strategy for the PM vessel subjected to loss of an MLBE and demonstrate that mooring line breakage is prevented.

5.1. Overview. A simulation was carried out using the Marine System Simulator (MSS) developed at the Norwegian University of Science and Technology (NTNU).

A turret-moored FPSO vessel model from the MSS library is used. The vessel dimensions are: length $L_{pp} = 200$ m, width $B = 44$ m, draught $T = 12$ m. The turret mooring system consists of 12 mooring lines with buoys shown in Figs. 6–7. The mooring length is $L = 2250$ m, the diameter is $D = 0.07$ m, the cable density is $\rho_c = 5500$ kg/m³, the added mass coefficient is $C_{mn} = 1.5$, the normal drag coefficient is $C_{dn} = 1$, and the tangential drag coefficient is $C_{dt} = 0.3$. A buoy is connected at position $s = 850$ m along an un-stretched mooring line from the terminal the point. The buoy is 8×10^4 kg with a volume of $V = 120$ m³. The added mass of the buoy is 5.8×10^4 kg and the drag force coefficient is $C_{dx} = 0.7$. The working water depth is 1000 m, and the mooring lines are simulated from a finite element model with RIFLEX software (MARINTEK, 2003). Each mooring line consists of 300 finite elements. From the touch point to the buoy there are 100 elements, and there are 200 elements from the buoy to the terminal point.

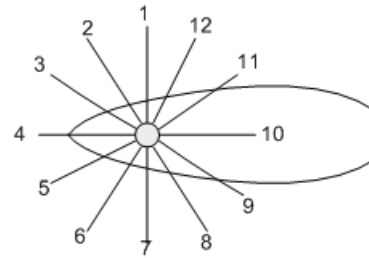


Fig. 6. Mooring system configuration with 12 lines.

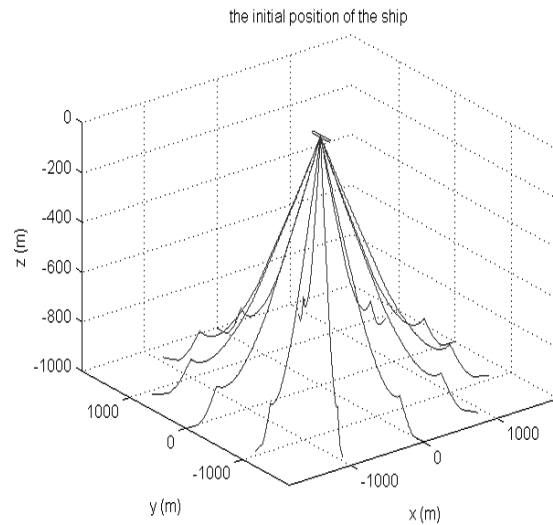


Fig. 7. Three dimensional illustration of a ship with mooring lines equipped with buoyancy elements.

A JONSWAP wave spectrum is used with a significant wave height of $H_s = 7$ m and a wave period of $T_p = 10.5$ s. The current is $v_c = 1$ m/s at the top and decreases to 0.2 m/s at a depth of 500 m. At the sea floor, the current is 0 m/s. The wind speed is $v_w = 8$ m/s and the wind direction is 45 deg. The environmental simulation on the vessel refers to Fossen (2002) and the current profile simulation to MARINTEK (2003).

5.2. Simulation with line breakage. In the presence of a strong sea current, mooring lines may have a high risk of breaking if not adequately assisted by thrusters. Nguyen *et al.* (2007) recommended to evaluate the external environment and then determine off-line a critical level of slowly-varying drift forces. After this, appropriate controls can be initiated to compensate for the increasing environmental forces according to the change of environment. The PM is limited in the region evaluated by a certain critical position defined off-line. Berntsen *et al.* (2008b) proposed a control strategy based on the structural reliability index. With this approach, the vessel moves in a safe region where the index is bigger than a critical value. However, this method is applied for only one critical mooring line. The optimal position algorithm proposed here utilises the mooring line tension for evaluation of external environmental effects and performs an on-line calculation of an optimal position to avoid line breakage. In addition, more than one critical mooring line can be protected.

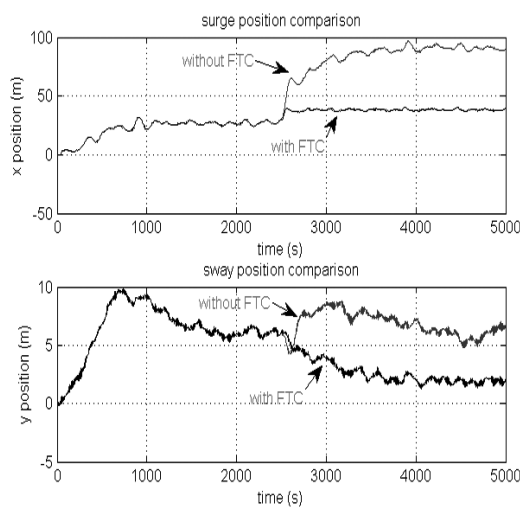


Fig. 8. Variation of position in the case of line breakage.

If one of the mooring lines is broken, there is another equilibrium point for the external environmental force that is acting. While moving towards a new equilibrium, there is a high possibility of getting beyond the critical tension for other mooring lines, causing breakage of other mooring lines. A simulation of this process is shown in Figs. 8–

10 when the No. 10 mooring line encounters a breakage at $t = 2500$ s.

From Figs. 10(e)–10(f), tensions in No. 9 and No. 11 mooring lines rapidly get beyond the critical mooring line tension $T_c = 2.0e6$ N, shown as the red straight line in the figures. No. 8 and No. 12 lines increase comparatively slowly and finally reach a critical value. This is avoided by the optimal position algorithm. With the algorithm, the tensions in No. 2–6 mooring lines are higher in the case without the optimal position algorithm, but they are kept below critical tension. The tension variation of No. 1 and No. 7 lines is quite small and also kept below the critical value.

Position deviation from the origin is shown in Fig. 8. The thruster force commanded is also shown in Fig.9. From Figs. 8 and 9, it is found that the thrusters contribute part of restoring force of the mooring system with the optimal position algorithm after mooring line breakage, and then PM comes into a new optimal set-point. This is consistent with our design target.

This simulation shows the case when more than one mooring line get beyond the critical tension. The optimal position algorithm proposed here can handle this common situation, while the structural reliability-based non-linear controller (Berntsen *et al.*, 2008b) could be applied on only one critical mooring line. A salient feature of the new algorithm is hence that there is no limit to the number of mooring lines that can be handled by the optimal position algorithm. The extent to which the features of this algorithm can be utilised depend on the availability of sufficient thruster forces.

5.3. Simulation with loss of a buoyancy element. The loss of a buoy is another event where mooring lines could get beyond critical tension in severe conditions.

A simulation with this event is shown in Figs. 11–13.

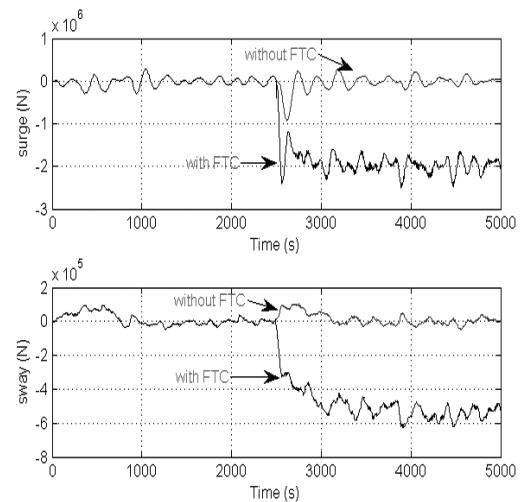


Fig. 9. Thruster force command in the case of line breakage.

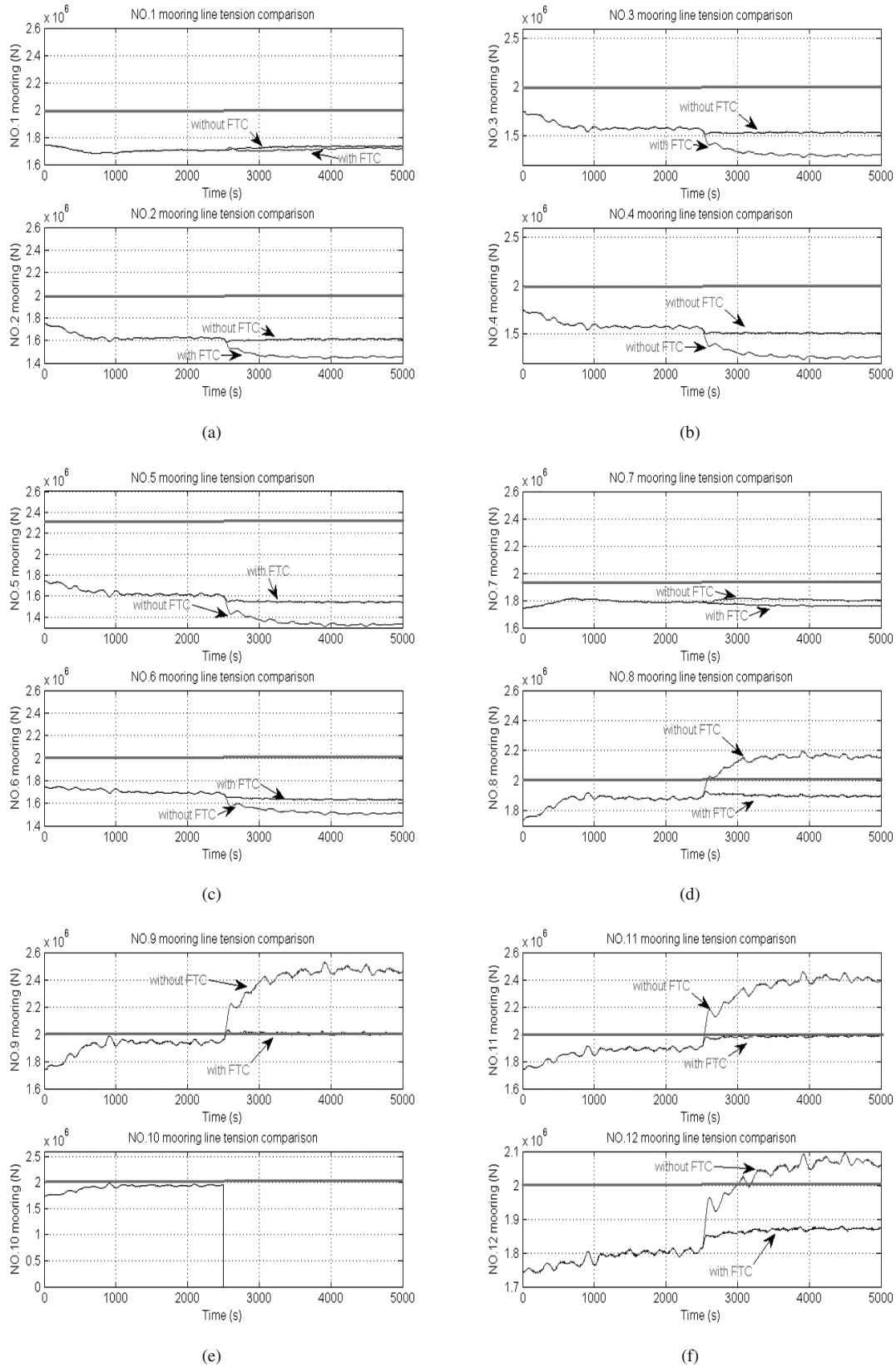


Fig. 10. Mooring line tensions in the case of breakage of line No. 10: lines 1 & 2 (a), lines 3 & 4 (b), lines 5 & 6 (c), lines 7 & 8 (d), lines 9 & 10 (e), lines 11 & 12 (f).

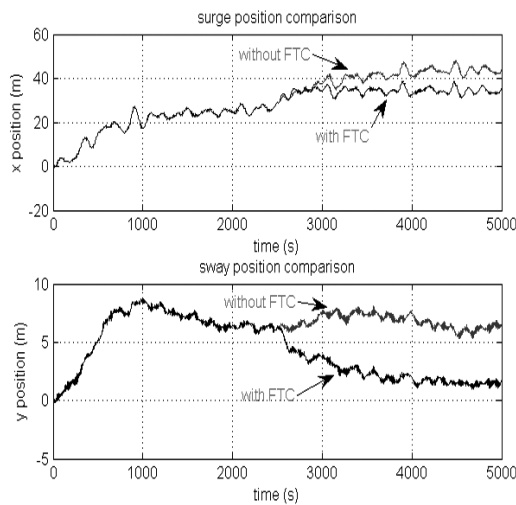


Fig. 12. Time variation of x and y positions with loss of the MLBE.

In this simulation, the tension of the No. 4 mooring line increases after the buoy is lost at $t = 2500$ s, and the mooring system comes into a new equilibrium where No. 4 mooring line is still within a safe range. However, the tensions of the mooring lines Nos. 9–11 are increased beyond the critical value with the loss of the MLBE in the No. 4 mooring line. The other lines are not critical as their tensions are well below the limit.

With the optimal position algorithm shown in Eqn. (9), PM moves to the optimal position after the loss of the MLBE on the No. 4 mooring line. The mooring lines No. 9–11 come close to critical tension, but the mooring system remains safe with all the other lines below critical tension. The position variation and thruster force commands are shown in Figs. 12 and 13, where more thruster effort is used after the loss of the MLBE and a new set-point is achieved. The algorithm can handle simultaneous faults and protect the position mooring system for more than one mooring line in danger of breakage.

6. Conclusion

Fault-tolerant control for position mooring was analysed in this paper with specific emphasis on the cases of loss of a mooring line buoyancy element and line breakage. Position-mooring control was analysed with the dynamics of mooring line buoys attached. Structural analysis was employed to get residuals to detect changes that could indicate faults in the system. A new fault-accommodating position algorithm was suggested that could prevent critical safety levels of mooring line tension from being exceeded. The proposed algorithm monitored the influence of the external environment directly from tensions of the

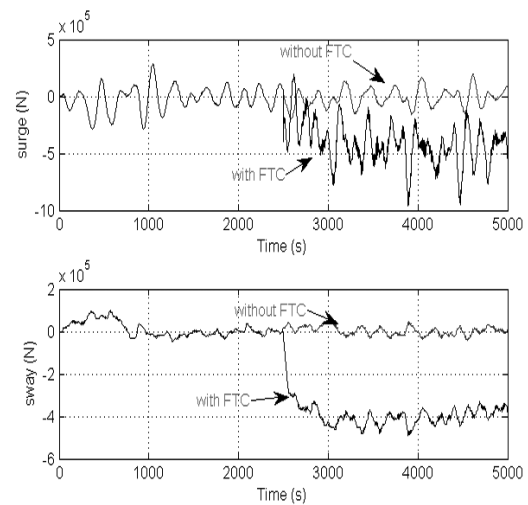


Fig. 13. Commanded thruster force with loss of the MLBE.

mooring lines, and the control algorithm was able to simultaneously control the tension of more than one mooring line, even when it was close to critical levels, provided sufficient thruster forces were available.

References

- Aamo, O. and Fossen, T. (2001). Finite element modelling of moored vessels, *Mathematical and Computer Modelling of Dynamical Systems* **7**(1): 47–75.
- Berntsen, P., Aamo, O. and Leira, B. (2006). Dynamic positioning of moored vessels based on structure reliability, *Proceedings of the 45th IEEE Control and Decision Conference, San Diego, CA, USA*, pp. 5906–5911.
- Berntsen, P., Aamo, O. and Leira, B. (2008a). Structural reliability-based control of moored interconnected structures, *Control Engineering Practice* **16**(4): 495–504.
- Berntsen, P., Aamo, O. and Leira, B. (2008b). Thruster assisted position mooring based on structural reliability, *International Journal of Control* **81**(9): 1408–1416.
- Blanke, M. (2005). Diagnosis and fault-tolerant control for ship station keeping, *Proceedings of the 13th Mediterranean Conference on Control and Automation, Limassol, Cyprus*, pp. 1379–1384.
- Blanke, M., Kinnaert, M., Lunze, J. and Staroswiecki, M. (2006). *Diagnosis and Fault-tolerant Control*, 2nd Edn., Springer, Berlin/Heidelberg.
- Blanke, M. and Staroswiecki, M. (2006). Structural design of systems with safe behaviour under single and multiple faults, *Proceedings of the IFAC Symposium SAFEPROCESS 2006, Beijing, PR China*, pp. 474–479.
- DNV (2008a). Dynamic positioning systems, *Rules for Classification of Ships*, Part 6, Chapter 7, Det Norsk Veritas, Oslo.
- DNV (2008b). Position mooring, *DNV-OS-E301*, Offshore Standard, Det Norsk Veritas, Oslo.

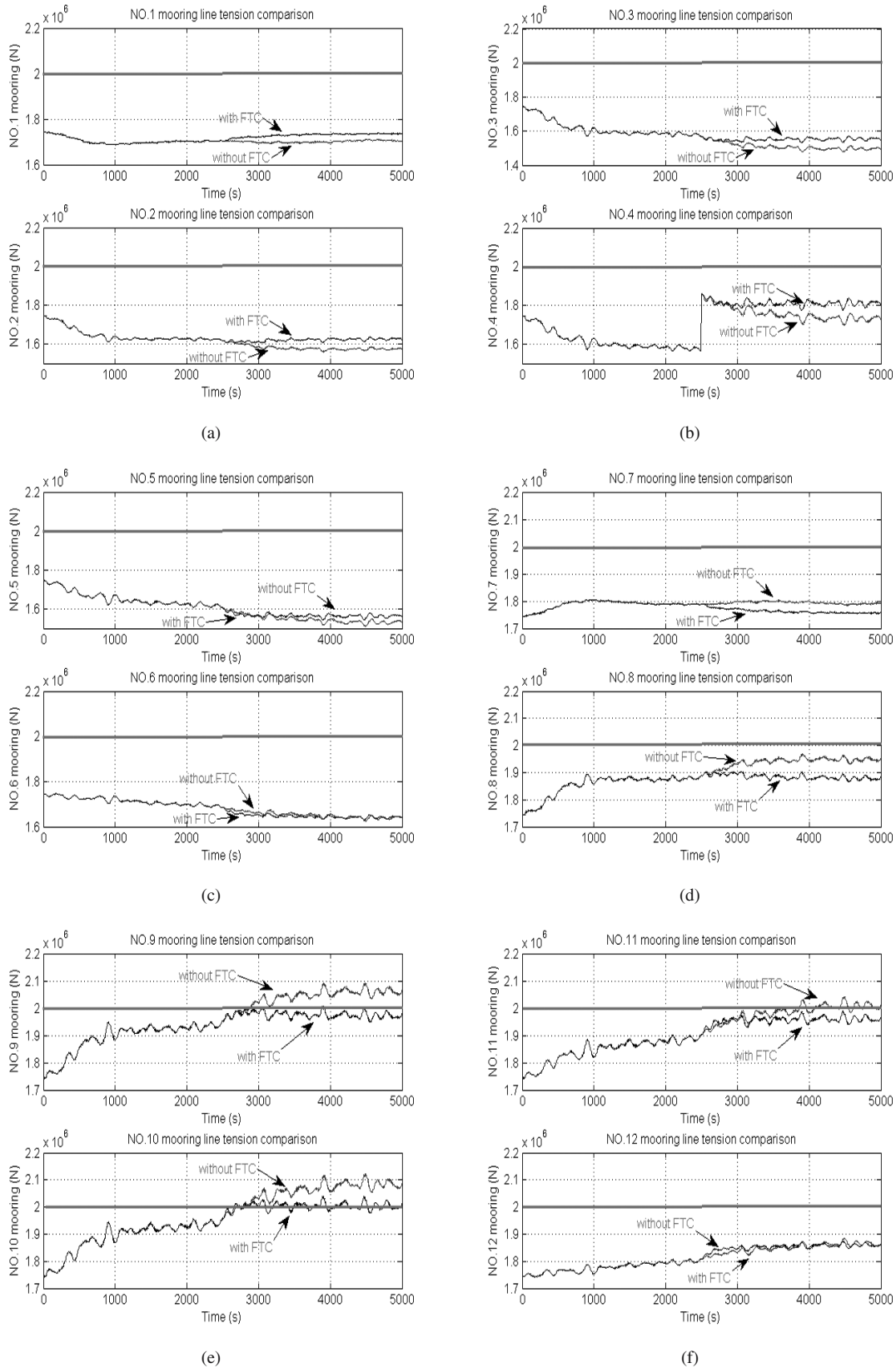


Fig. 11. Mooring line tensions with loss of a buoyancy element on line No. 4: lines 1 & 2 (a), lines 3 & 4 (b), lines 5 & 6 (c), lines 7 & 8 (d), lines 9 & 10 (e), lines 11 & 12 (f).

- Fossen, T.I. (2002). *Marine Control System*, Marine Cybernetics, Trondheim.
- Gao, Z. and Moan, T. (2007). Sensitivity study of extreme value and fatigue damage of line tension in mooring system with one line failure under varying annual environmental condition, *Proceedings of the 17th International Offshore and Polar Engineers Conference (ISOPE)*, Lisbon, Portugal, pp. 3753–3760.
- Garza-Rios, L.O. and Bernitsas, M.M. (1996). Analytical expressions of the stability and bifurcation boundaries for general spread mooring systems, *Journal of Ship Research* **40**(4): 337–350.
- Kay, S. (1998). *Fundamentals of Statistical Signal Processing, Volume 2: Detection Theory*, Prentice Hall, Upper Saddle River, NJ.
- Kim, M. and Dick, K. (1989). Slowly-varying wave drift forces in short-crested irregular seas, *Applied Ocean Research* **11**(1): 2–18.
- Laursen, M., Blanke, M. and Dustegor, D. (2008). Fault diagnosis of a water for injection system using enhanced structural isolation, *International Journal of Applied Mathematics and Computer Science* **18**(4): 593–603, DOI: 10.2478/v10006-008-0052-5.
- MARINTEK (2003). RIFLEX User Manual, *MARINTEK report no. 519619*, Trondheim.
- Mavrakos, S., Papazoglou, V., Triantafyllou, M. and Hatjigeorgiou, J. (1996). Deep water mooring dynamics, *Marine Structure* **9**(2): 181–209.
- Næss (1986). The statistical distribution of the second order slowly varying forces and moments, *Applied Ocean Research* **8**(2): 110–118.
- Nguyen, D., Blanke, M. and Sørensen, A. (2007). Diagnosis and fault-tolerant control for thruster-assisted position mooring, *Proceedings of the IFAC Conference on Control Applications in Marine Systems, CAMS'2007, Bol, Croatia*, DOI: 10.3182/20070919-3-HR-3904.00051.
- Nguyen, D. and Sørensen, A. (2007). Setpoint chasing for thruster-assisted position mooring, *Proceeding of the 26th International Conference of Ocean, Offshore and Arctic Engineering (OMAE)*, San Diego, CA, USA, pp. 553–560.
- Nguyen, D. and Sørensen, A. (2009). Switched control for thruster-assisted position mooring, *Control Engineering Practice* **17**(9): 985–994.
- Nguyen, D.T. and Blanke, M. (2009). Fault-tolerant positioning control for offshore vessels with thruster and mooring actuation, *Technical report*, Norwegian University of Technology and Science, CeSOS, Trondheim.
- Poulsen, N.K. and Niemann, H. (2008). Active fault diagnosis based on stochastic tests, *International Journal of Applied Mathematics and Computer Science* **18**(4): 487–496, DOI: 10.2478/v10006-008-0043-6.
- Strand, J., Sørensen, A. and Fossen, T. (1998). Design of automatic thruster assisted position mooring systems for ships, *Modelling, Identification and Control* **19**(2): 61–75.
- Tomera, M. (2010). Nonlinear controller design of a ship autopilot, *International Journal of Applied Mathematics and Computer Science* **20**(2): 271–280, DOI: 10.2478/v10006-010-0020-8.
- Wang, K. and Xu, W. (2008). Study of wave drift forces affecting FPSO systems, *Harbin Gongcheng Daxue Xuebao/Journal of Harbin Engineering University* **29**(12): 1261–1265.
- Wang, Y.-G. and Tan, J.-H. (2008). Markov modeling for slow drift oscillations of moored vessels in irregular waves, *Chuan Bo Li Xue/Journal of Ship Mechanics* **12**(3): 368–376.
- Witkowska, A., Tomera, M. and Śmierczalski, R. (2007). A backstepping approach to ship course control, *International Journal of Applied Mathematics and Computer Science* **17**(1): 73–85, DOI: 10.2478/v10006-007-0007-2.



Shaoji Fang is a Ph.D. student at the Norwegian University of Technology and Science, NTNU, in Trondheim. He received his M.Sc. from Harbin Engineering University in 2006. He was a systems engineer at J. Ray Mcdermott Asian Pacific in the years 2007–2008. His research is focused on reliable and fault-tolerant control of marine vessels.



Mogens Blanke is a professor of automation and control at the Technical University of Denmark. His research interests include autonomous fault-tolerance, fault-diagnosis, systems architecture design to obtain desired safety properties, system modelling, identification and control. M. Blanke had a role in developing the area of fault-tolerant control in Europe, demonstrating both ideas towards a methodology in the area and applications of the theory to satellite attitude control and marine automation. M. Blanke is the technical editor for fault-tolerant systems for *IEEE Transactions of Aerospace and Electronic Systems* and an associate editor for *Control Engineering Practice*. He was the founder of the IFAC Technical Committee of Marine Systems in 1987, has held other IFAC positions and was a member of the IFAC Council from 1997 till 2000. His honorary positions include a visiting professor at Dalian Maritime University (since 2000), a member of the Danish Academy of Technical Sciences (since 2001), and a research adjunct professor at NTNU in Trondheim (since 2004).

Received: 1 March 2010

Revised: 20 November 2010